DOT/FAA/AR-11/1,P3

Federal Aviation Administration
William J. Hughes Technical Center
Aviation Research Division
Atlantic City International Airport
New Jersey 08405

Adhesively Bonded Joints

Part 3: Effect of Bondline Thickness on Mixed Mode Fracture of Adhesively Bonded Joints

February 2014

Final Report

This document is available to the U.S. public through the National Technical Information Services (NTIS), Springfield, Virginia 22161.

This document is also available from the Federal Aviation Administration William J. Hughes Technical Center at actlibrary.tc.faa.gov.

U.S. Department of Transportation
Federal Aviation Administration

NOTICE

This document is disseminated under the sponsorship of the U.S. Department of Transportation in the interest of information exchange. The U.S. Government assumes no liability for the contents or use thereof. The U.S. Government does not endorse products or manufacturers. Trade or manufacturers' names appear herein solely because they are considered essential to the objective of this report. The findings and conclusions in this report are those of the author(s) and do not necessarily represent the views of the funding agency. This document does not constitute FAA policy. Consult the FAA sponsoring organization listed on the Technical Documentation page as to its use.

This report is available at the Federal Aviation Administration William J. Hughes Technical Center's Full-Text Technical Reports page: actlibrary.tc.faa.gov in Adobe Acrobat portable document format (PDF).

Technical Report Documentation Page

1. Report No.	2. Government Accession No.	3. Recipient's Catalog No.
DOT/FAA/AR-11/1,P3		

4. Title and Subtitle	5. Report Date
ADHESIVELY BONDED JOINTS, PART 3: EFFECT OF BONDLINE THICKNESS ON THE MIXED MODE FRACTURE OF ADHESIVELY BONDED JOINTS	August 2011
	6. Performing Organization Code
7. Author(s)	8. Performing Organization Report No.
Hyonny Kim	
9. Performing Organization Name and Address	10. Work Unit No. (TRAIS)
Purdue University 155 S. Grant Street West Lafayette, IN 47907	
	11. Contract or Grant No.
12. Sponsoring Agency Name and Address	13. Type of Report and Period Covered
U.S. Department of Transportation Federal Aviation Administration Aviation Safety Aircraft Certification Service—Aircraft Engineering Division 1601 Lind Ave., SW Renton, WA 98057	Final Report 2004-2010
	14. Sponsoring Agency Code AIR-100

15. Supplementary Notes

The Federal Aviation Administration William J. Hughes Technical Center Aviation Research Division Technical Monitor was Lynn Pham.

16. Abstract

This report details work conducted at Purdue University under the Federal Aviation Administration (FAA) Joint Advanced Materials and Structures Center of Excellence program advancing knowledge on adhesively bonded structures and addresses the issues of the correlation between bondline thickness and fracture, as well as the design of hybrid adhesively bonded joints. This report is one of three reports that were generated by the FAA program.

The effect of bondline thickness on the critical strain energy release rate at fracture initiation for different modes of loading was investigated. A complete fracture envelope was developed for different adhesive thicknesses and is reported herein. The measurement of the fracture envelope was carried out by employing double cantilever beam, mixed-mode bending (MMB) and end notch flexure test methods. It was found that the bondline thickness affects the critical strain energy release rate (CSRR) for different amounts of mode II component. Pure mode II dissipated the most energy and, consequently, had the largest CSRR, whereas pure mode I had the least. The shape and size of the plastic zone developed prior to the onset of propagation was also investigated by numerical analysis. It was found that the variation of CSRR as a function of adhesive thickness can be related to the size of the developed plastic zone for mode I and MMB 50% fracture. With the increasing amount of mode II content beyond 50% ratio, no correlation was observed due to the development of a large plastic zone throughout most of the adhesive volume.

17. Key Words	18. Distribution Statement
Adhesively bonded joints, Thickness effects, Mode I, Mode II, Mixed mode, Fracture mechanics, Fracture testing, Plastic zone	This document is available to the U.S. public through the National Technical Information Service (NTIS), Springfield, Virginia 22161. This document is also available from the Federal Aviation Administration William J. Hughes Technical Center at actlibrary.tc.faa.gov.

19. Security Classif. (of this report)	20. Security Classif. (of this page)	21. No. of Pages	22. Price
Unclassified	Unclassified	27	

Form DOT F 1700.7 (8-72) Reproduction of completed page authorized

TABLE OF CONTENTS

		Page
EXECUTIVE SUMMARY		vi
1.	INTRODUCTION	1
2.	EXPERIMENTS	2
2.1	Specimen Description and Surface Preparation	2
2.2	Bonding Procedure	3
2.3	Mechanical Tests	4
2.4	Experimental Setup	5
3.	RESULTS	5
3.1	Images of Adhesive Deformations Ahead of Crack Tip	5
3.2	Fracture Surfaces	8
3.3	Critical Strain Energy Release Rate Results	9
4.	FINITE ELEMENT ANALYSIS	13
4.1	Model Development	13
4.2	The FEA Results	13
5.	DISCUSSION	15
6.	CONCLUSIONS	17
7.	REFERENCES	18

LIST OF FIGURES

Figure		Page
1	Test Specimen Details and Tooling Assembly	3
2	Test Specimen Configurations	5
3	Loading History for Pure Mode I Test With 1.02-mm Bondline Thickness	6
4	Loading History for MMB 50% Test With 1.02-mm Bondline Thickness	6
5	Loading History for MMB 75% Test With 1.02-mm Bondline Thickness	7
6	Loading History for Pure Mode II Test With 1.02-mm Bondline Thickness	7
7	Fracture Surfaces for Pure Mode I, MMB 50%, MMB 75%, and Pure Mode II	8
8	Pure Mode I CSERR vs. Adhesive Thickness	10
9	The MMB 50% CSERR vs. Adhesive Thickness	11
10	The MMB 75% CSERR vs. Adhesive Thickness	11
11	Pure Mode II CSERR vs. Adhesive Thickness	12
12	The CSERR vs. Mixed-Mode Ratio for Different Thicknesses	12
13	Comparison of Plastic Zone Size and Shape for DCB Pure Mode I	14
14	Comparison of Plastic Zone Size and Shape for MMB 50%	14
15	Comparison of Plastic Zone Size and Shape for MMB 75%	15
16	Comparison of Plastic Zone Size and Shape for ENF Pure Mode II	15

LIST OF SYMBOLS AND ACRONYMS

G_{I_C}	Pure mode I CSERR
G_{II_C}	Pure mode II CSERR
CLS	Cracked lap shear
CMM	Compact mixed mode
CSERR	Critical strain energy release rate
DCB	Double cantilever beam
ENF	End notched flexure
FAA	Federal Aviation Administration
FEA	Finite element analysis
FPL	Forestry Product Laboratory
MMB	Mixed-mode bending
SERR	Strain energy release rate

EXECUTIVE SUMMARY

This report details work conducted at Purdue University under the Federal Aviation Administration (FAA) Joint Advanced Materials and Structures Center of Excellence program advancing knowledge on adhesively bonded structures and addresses the issues of the correlation between bondline thickness and fracture, as well as the design of hybrid adhesively bonded joints. This report is one of three reports that were generated by the FAA program.

The majority of the in-service adhesively bonded joints rarely encounter pure mode I or pure mode II loading. Thus, understanding thickness effects on adhesively bonded joint fracture toughness in the mixed-mode regime is crucial. Most efforts by previous researchers investigated the thickness effect of simple loading, such as pure mode I or pure mode II. No investigation efforts were found to generate critical strain energy release rate (CSERR) data for adhesively bonded joints in the mixed-mode (combination of mode I and mode II) regime. The current investigation is an expansion of previous work. Additional fracture data for adhesively bonded joints in the mixed-mode regime were collected to define the mixed-mode I/II fracture envelope and to assist in the understanding of adhesively bonded joint fracture behavior. The objectives of this research were to investigate the effect of various adhesive thicknesses on the CSERR of adhesively bonded joints for a range of mixed-mode ratios and to examine the relationship between finite element analysis-determined plastic zone size and shape to the experimentally measured fracture data.

The effect of bondline thickness on the CSERR at fracture initiation for different modes of loading was investigated. A complete fracture envelope was developed for different adhesive thicknesses and is reported herein. The measurement of the fracture envelope was carried out by employing double cantilever beam, mixed-mode bending (MMB) and end notch flexure test methods. It was found that the bondline thickness affects the CSERR for different amounts of mode II component. Pure mode II dissipated the most energy and, consequently, had the largest CSERR, whereas pure mode I had the least. The shape and size of the plastic zone developed prior to the onset of propagation was also investigated by numerical analysis. It was found that the variation of CSERR as a function of adhesive thickness can be related to the size of the developed plastic zone for mode I and MMB 50% fracture. With the increasing amount of mode II content beyond 50% ratio, no correlation was observed due to the development of a large plastic zone throughout most of the adhesive volume.

1. INTRODUCTION.

The majority of the in-service adhesively bonded joints rarely encounter pure mode I or pure mode II loading. Thus, understanding thickness effects on adhesively bonded joint fracture toughness in the mixed-mode regime is crucial. Most efforts by previous researchers investigated the thickness effect of simple loading, such as pure mode I or pure mode II. No investigation efforts were found to generate critical strain energy release rate (CSERR) data for adhesively bonded joints in the mixed-mode (combination of mode I and mode II) regime. The current investigation is an expansion of previous work. Additional fracture data for adhesively bonded joints in the mixed-mode regime were collected to define the mixed-mode I/II fracture envelope and to assist in the understanding of adhesively bonded joint fracture behavior. The objectives of this research were to investigate the effect of various adhesive thicknesses on the CSERR of adhesively bonded joints for a range of mixed-mode ratios and to examine the relationship between finite element analysis (FEA)-determined plastic zone size and shape to the experimentally measured fracture data.

Research showed that the failure properties, including the CSERR, of adhesively bonded joints varies with the adhesive thickness. This dependency was found to have different trends for different adhesive systems. Kinloch, et al. [1 and 2], correlated the fracture toughness of joints and the bulk adhesive with the size of the plastic zone developed inside the adhesive layer in pure mode I with different loading speeds. Kinloch hypothesized that the variability in fracture toughness of adhesively bonded joints is caused by the confinement of the plastic zone developed in the adhesive layer for different adhesive thicknesses. Kinloch further reported that when the bondline thickness is much larger than the plastic zone size, the CSERR will be the same as the fracture toughness of a bulk adhesive specimen. Hunston, et al. [3], further examined the hypothesis of Kinloch, et al. [1 and 2], studying whether the fracture behavior is related to the physical constraints of the developing plastic zone inside the adhesive by judging the dimension of the deformation zone from the stress whitening occurring at the crack tip. Chai [4] studied the effect of bondline thickness on mode I, mode II, and mode III fractures with different particle size, distribution, and hardness. Chai reported that all fracture energies of different modes of loading converge to a single value when the bondline thickness is in the micron length scale. In this study, he found that G_{I_C} and G_{II_C} increase with thickness and then level off. He also found that the plastic zone ahead of the crack tip may exceed 1000 times the dimension of the bond thickness. Chai also investigated the effect of adhesive thickness for different adhesive systems [4 and 5]. Chai found that not all adhesives exhibit an adhesive thickness dependency effect and different adhesive systems produce different trends of CSERR. He also concluded that the reduction in toughness with decreased thickness is due to the adherends over-constraining the plastic zone ahead of the crack tip [5].

In the mixed-mode regime, different test methodologies, including mixed-mode bending (MMB), cracked lap shear (CLS), scarf joints, and compact mixed mode (CMM), were employed by various authors. Benzeggagh and Kenane [6] and Ducept, et al. [7], studied the mixed-mode delamination of glass/epoxy composite. Double cantilever beam (DCB) and mixed-mode bending (MMB) were employed in both studies to generate the pure mode I and mixed-mode fracture envelopes. However, reference 6 employed end-loaded split specimens, whereas

reference 7 employed end-notched flexure (ENF) to generate the fracture data for pure mode II loading. Semi-empirical criterion for the whole regime of mixed-mode fracture was developed in reference 6. Reference 7 also looked into the mixed-mode fracture of adhesively bonded composite joints and found that the fracture energies are much higher for bonded joints than the composite material specimens alone (e.g., the delamination between plies).

Efforts of generating the mixed-mode fracture envelope were performed for polymer-matrix composite materials [6 and 7] and for adhesively bonded joints with a single bondline thickness [7]. Mode II fracture of adhesively bonded joints were investigated extensively by Chai [8-13]. Thickness varying from very thin (1 µm) to a range great enough (0.5 mm) to reveal the bulk fracture behavior was investigated [8]. A high-magnification video camera was used to monitor the adhesive shear strain using vertical scratch marks on the specimen edge. Chai also derived a strain energy release rate analytical model that considered the adhesive nonlinear behavior [10] and related the fracture criterion of joints to the ultimate shear strain of the adhesive [11]. Chai further investigated the failure process of adhesively bonded joints under mode II fracture with scanning electron microscopy and concluded that the decline of ultimate shear strain with decreasing adhesive thickness was caused by tensile microcracks that were formed in the interlayer during loading [11]. In reference 14, an analytical model of the shear stress distribution along the crack tip for different adhesive thicknesses was derived and then validated these models by FEA. These authors performed experiments with compact pure shear test specimens and concluded that G_{II_C} rose sharply for very small bond thickness (0.02 mm) and increased gradually for larger bond thickness (0.9 mm). A constraint effect of the adherend, which suppressed and prevented the plastic zone from growing for small bondline thickness, was hypothesized. Their conclusion was that an adhesively bonded joint is tougher in shear than in tension.

2. EXPERIMENTS.

2.1 SPECIMEN DESCRIPTION AND SURFACE PREPARATION.

Aluminum alloy 2024-T3 (25.4 mm wide, 203 mm long, and 6.35 mm thick) was used as the adherend material. Two 3.97-mm through holes were drilled 6.3 mm from each end. The holes served to ensure that the two adherends were properly aligned to each other by using dowel pins during joint assembly and curing, as shown in figure 1.

The aluminum adherend surface must undergo proper surface preparation to prevent the joint from experiencing adhesion failure (clean separation at the adhesive-aluminum interface). The bond durability is significantly enhanced when the adherend surface contains a significant degree of microscopic roughness. This microrough morphology provides mechanical locking between the adhesive and the oxide layer on the aluminum adherend [15]. The Forest Products Laboratory (FPL) chemical etching surface preparation procedure for aluminum adherends [15] was used for the adhesive bonding in this project. The bonding surface was first sanded prior to chemical etching to ensure that the dirt and grease on the aluminum surface were removed so that the chemical etchant could thoroughly react with the aluminum surface. Sandpaper of 100 grit was used to remove the grease and dirt on the surface, followed by 200-grit sandpaper to provide

a smoother bonding surface. The aluminum adherends were then soaked in a bath of isopropyl alcohol for 5 minutes before being wiped thoroughly using lint-free tissues. The adherends were left in the open air to dry for approximately 5 minutes after cleaning. Semco® Pasa-Jell 105, a chromic-sulfuric acid etchant (supplied by FPL) used as an aluminum surface pretreatment, was applied thoroughly on the entire bonding surface and left in the ventilation hood for 15 minutes, as recommended by the manufacturer. The Pasa-Jell was then removed with lint-free tissues, and the adherends were rinsed in tap water for 5 minutes. Deionized water was used as a final rinse of the bonding surfaces. The specimens were subsequently dried in the oven for 15 minutes at 82°C.

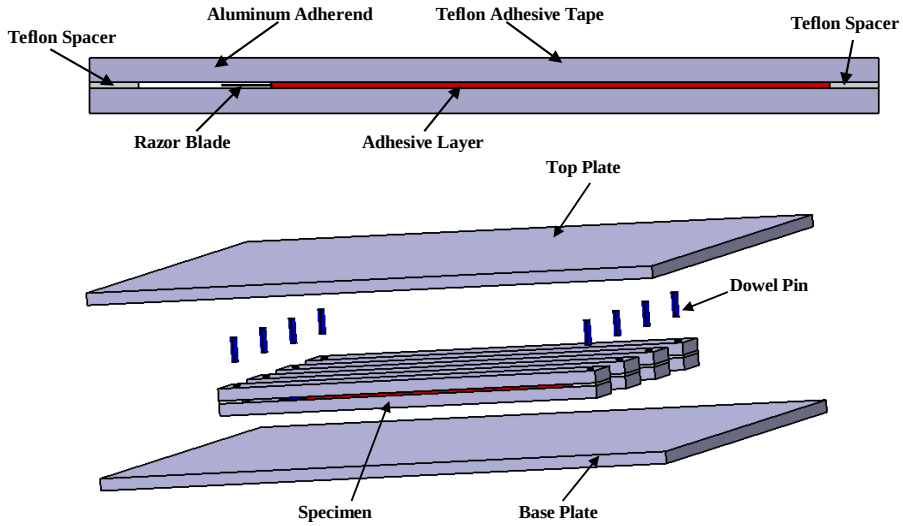

Figure 1. Test Specimen Details and Tooling Assembly

2.2 BONDING PROCEDURE.

A 0.254-mm-thick razorblade was used as the crack starter, as shown in figure 1. Teflon® sheets were stacked on both sides of the razorblade so that their overall stack thickness was equal to the desired adhesive thickness. Taking care not to contaminate the adherends, mold release agent was spray-coated onto the razorblade to allow them to be removed from the crack tip after the adhesive cure. The release coating was allowed to dry for roughly 5 minutes before any excess release agent buildup was gently wiped off the razorblade to prevent contamination of the adhesive. The razorblade was attached to the aluminum adherend at a desired location, thereby defining a specific initial crack length, using cyanoacrylate adhesive.

The adhesive system used in this project was PTM&W Industries, Inc. ES6292 two-part paste epoxy. The resin was mixed with the hardener at the mass ratio of 100:31.5, as specified by the manufacturer. The resin was combined with the hardener and thoroughly stirred with a mixing stick for 2 minutes. A horsehair brush was used to apply the adhesive onto the aluminum adherend surfaces. The adhesive on the horsehair brush was firmly dabbed onto the adherend surface to ensure that the adhesive adequately penetrated the microrough oxide layer produced by the FPL etch treatment, thereby establishing a mechanical interlock with the adherend surface. Extra adhesive was then applied on both bonding surfaces; the two adherends were assembled

between two 6.35-mm-thick aluminum tool plates, as shown in figure 1, and placed into a hydraulic press. Alignment of the two adherends during assembly and compaction was achieved by the dowel pins (see figure 1) inserted through the predrilled holes on each adherend. Teflon sheets were used as spacer shims to control the desired adhesive thickness.

All specimens were cured at room temperature for 12 hours per the manufacturer's specification while held in the hydraulic press. The specimens were then postcured in an oven at 82°C for 5 hours per manufacturer specification. The postcuring process was necessary to obtain improved adhesive properties. After postcuring, the previously mentioned dowel pin alignment holes near the adherend ends were threaded with a #10-32 unified fine thread tap to allow the loading hinges to be fastened onto the specimen. A paper rule with 1.59-mm-scale line spacing was attached to the edge of the crack tip to aid in crack length measurements. A sharp razorblade and a precision L-square were used to define scribe lines on the side of the specimen, crossing the adhesive layer. These lines were monitored by a video microscope during loading to directly observe the degree of plastic strain developed in the adhesive layer.

2.3 MECHANICAL TESTS.

The DCB test method, shown in figure 2(a), was used extensively to determine the strain energy release rate (SERR) of pure mode I fracture, i.e., G_{I_C}, as specified by ASTM D 3433 [16], and has been used by many researchers [4, 6, 7, 17, and 18]. The MMB test method, shown in figure 2(b), was used to determine the CSERR for a wide range of mixed-mode I and II ratio fractures, as specified by ASTM D 6671 [19]. This test was used in references 6 and 7 to study delamination of polymer-matrix composite materials over the entire mixed-mode envelope (i.e., various ratios of modes I and II). The basic idea of this test method was to combine the mode I DCB and the mode II ENF test (see ENF in figure 2(c)) into a configuration in which a single load can be applied to obtain different combinations of mixed-mode ratio [20]. The mixed-mode ratio can be defined by adjusting the lever arm length, c [19], as indicated in figure 2(b). ENF is a three-point loaded test method used to determine the SERR for pure mode II fracture. This test was employed by Chai [9-13] to study the effect of adhesive thickness on pure mode II fracture of adhesively bonded joints. These three test methods were chosen for this project because the same specimen geometry can be used with any of the three test fixtures to obtain a complete mixed-mode I/II CSERR envelope.

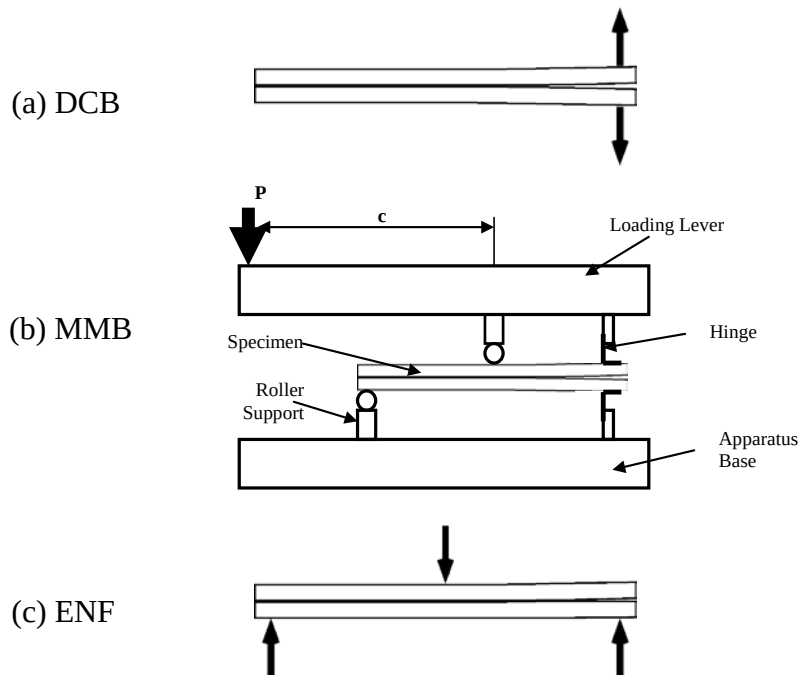

Figure 2. Test Specimen Configurations

2.4 EXPERIMENTAL SETUP.

A 100-kN material test machine (MTS 810) was used for all fracture tests. Other equipment, such as a long-distance microscope (Infinity Photo-Optical Co. model K2/SC™), was used for observing the events of pre- and postfracture processes in the vicinity of the crack tip; and a laser extensometer was used to measure the beam opening displacement of mode I, MMB 50%, and MMB 75% fracture tests, where the mode mix ratio (in percent) is defined as the ratio of mode II component to the total, i.e., $G_{II}/(G_I+G_{II})$. Load, actuator displacement, and beam-opening displacement data were recorded. A laser extensometer (Electronic Instrument Research LE-05) was used to directly measure the beam-opening displacements at the applied load points where reflective tape strips had been applied, and thus, this displacement measurement scheme was not affected by compliance from the test fixtures and the test machine itself. Crack tip region images were captured with a 6.6-mega-pixel PixeLINK® PL-781 digital camera.

3. RESULTS.

3.1 IMAGES OF ADHESIVE DEFORMATIONS AHEAD OF CRACK TIP.

Sequential images of the crack tip region were captured by the long-distance microscope while loading was applied. The sequential images of different mixed-mode ratio conditions for joints having 1.02-mm adhesive thickness are shown in figures 3 through 6. The boxed numbers on the load-displacement curve corresponds to the deformation images at that particular time. Image 1 always shows the specimen's initial state before any loading was applied. The vertical lines visible in the images are the aforementioned scribe lines that show the amount of shear deformation developed in the adhesive during the test.

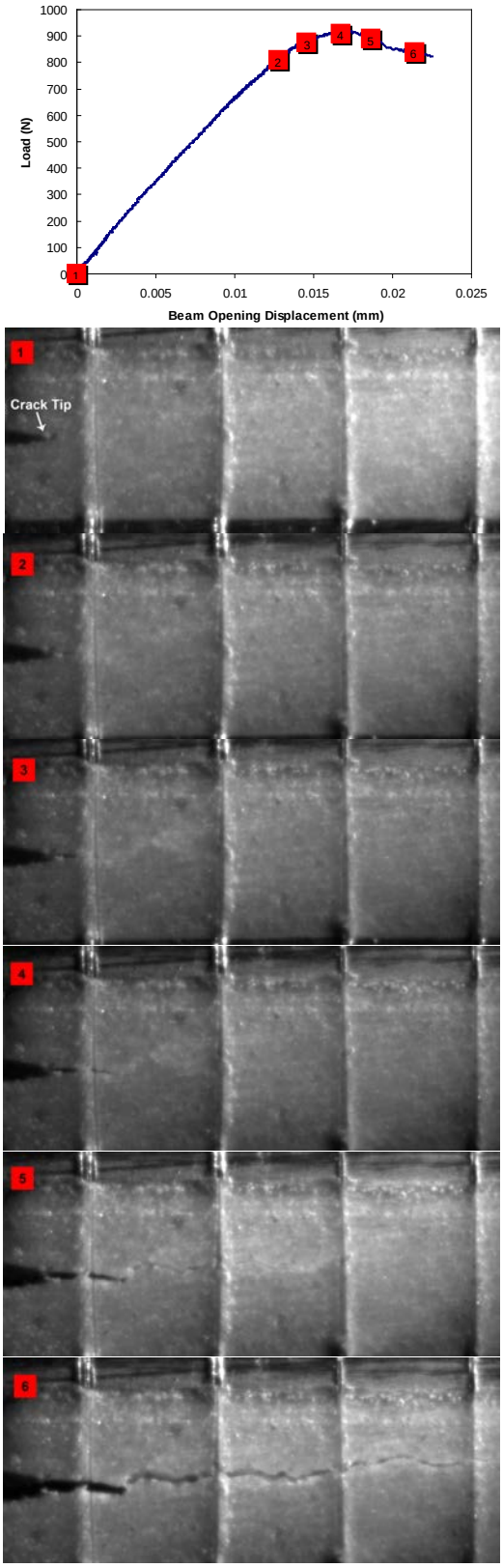

Figure 3. Loading History for Pure Mode I Test With 1.02-mm Bondline Thickness

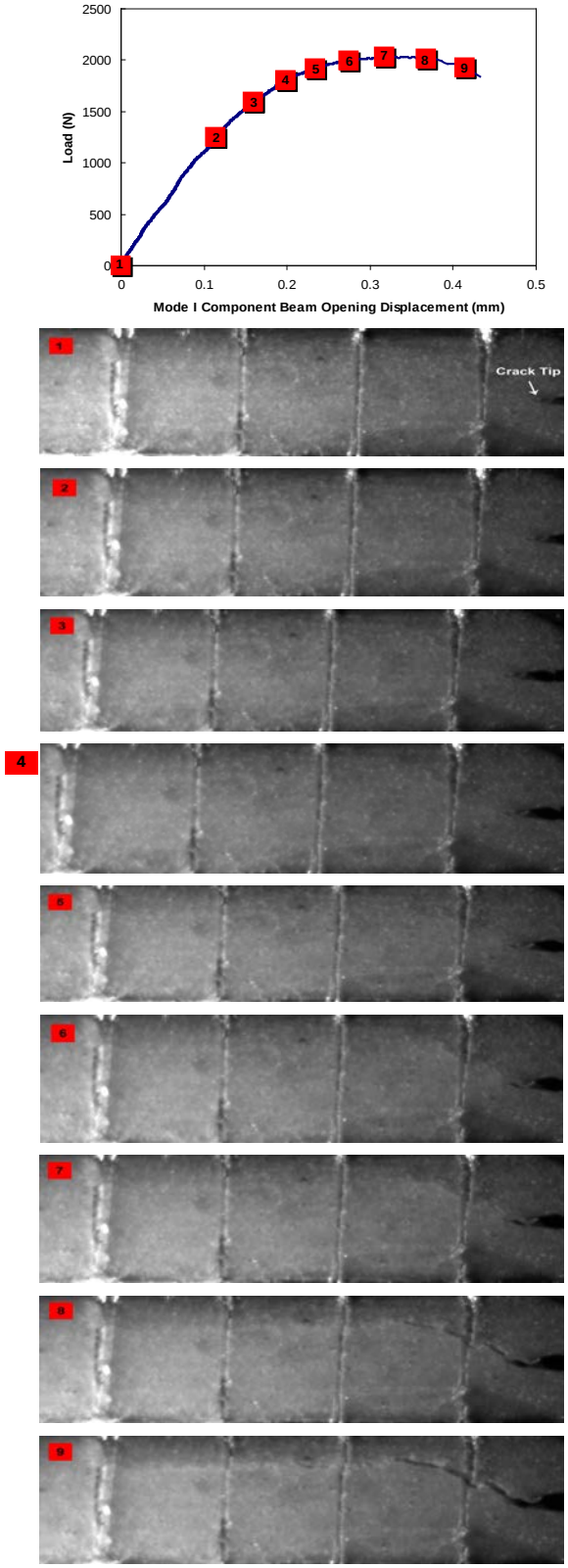

Figure 4. Loading History for MMB 50% Test With 1.02-mm Bondline Thickness

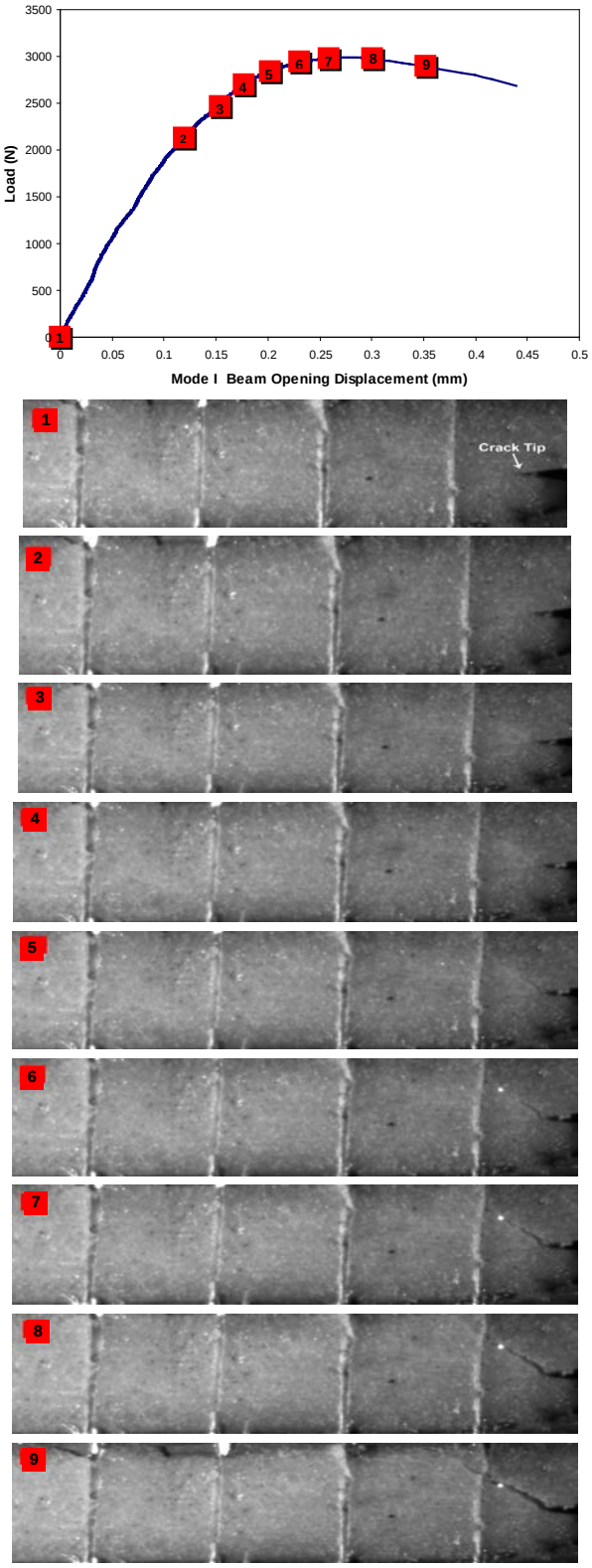

Figure 5. Loading History for MMB 75% Test With 1.02-mm Bondline Thickness

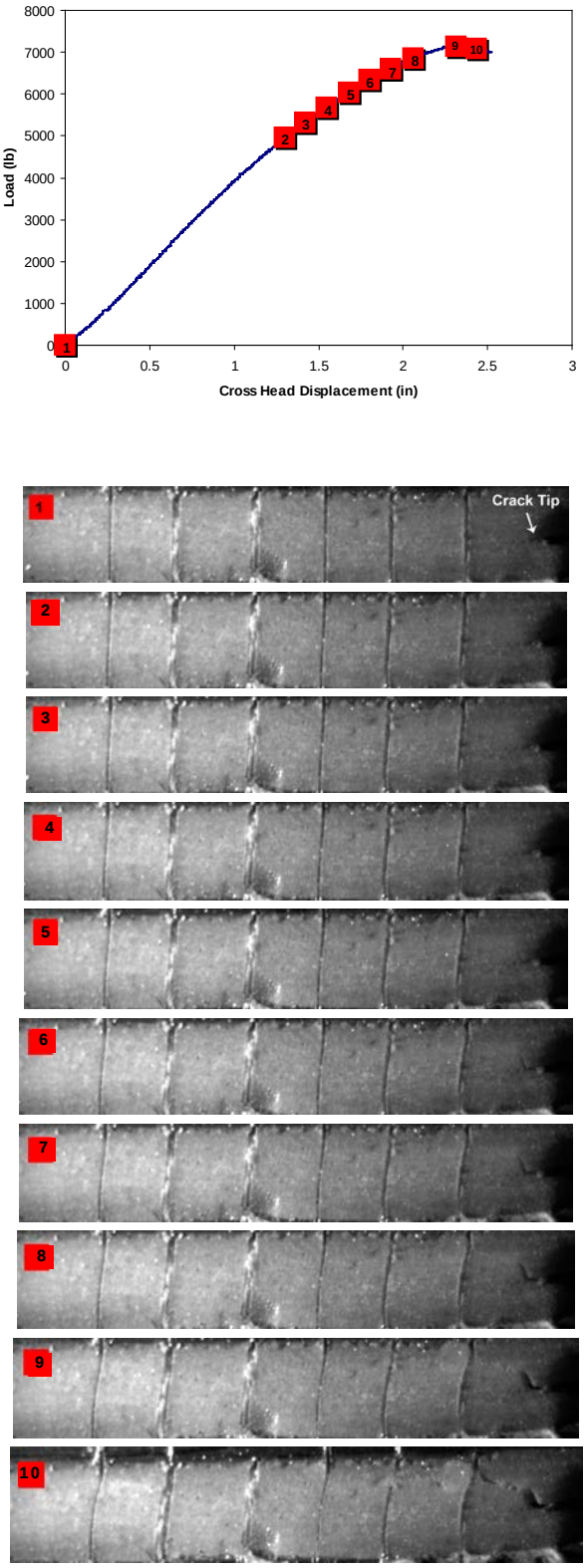

Figure 6. Loading History for Pure Mode II Test With 1.02-mm Bondline Thickness

3.2 FRACTURE SURFACES.

The fracture surfaces of the adhesively bonded joint can generally be categorized into cohesive failure, adhesion failure, and substrate failure [21]. However, only cohesive and adhesion failures were encountered throughout these experiments due to the aluminum adherends being much stiffer and tougher than the polymer adhesive. The cohesive failure mode describes a fracture that occurs completely within the adhesive layer. Adhesion failure describes a fracture that occurs cleanly between the adhesive and adherend. Cohesive failure is the desired failure mode to determine the fracture energy of the adhesive [8]. The behavior of the load displacement curves for loading mode can be explained by fracture surfaces. Different fracture surfaces were encountered throughout the experiments. However, only specimens with cohesive failure surface were considered valid tests. Cohesive failure fracture surface of pure mode I fracture, mixed-mode fractures of 50% and 75%, and pure mode II are shown in figure 7. The specimens that experienced adhesion failure were not included in the data set because those are measurements of adhesion fracture energy instead of the adhesive properties. The adhesion fracture load is always lower than cohesive failure fracture load. The root causes of adhesion failure are attributed to inadequate surface preparation, namely, aluminum adherend surface not cleaned thoroughly, and/or incorrect chemical etching.

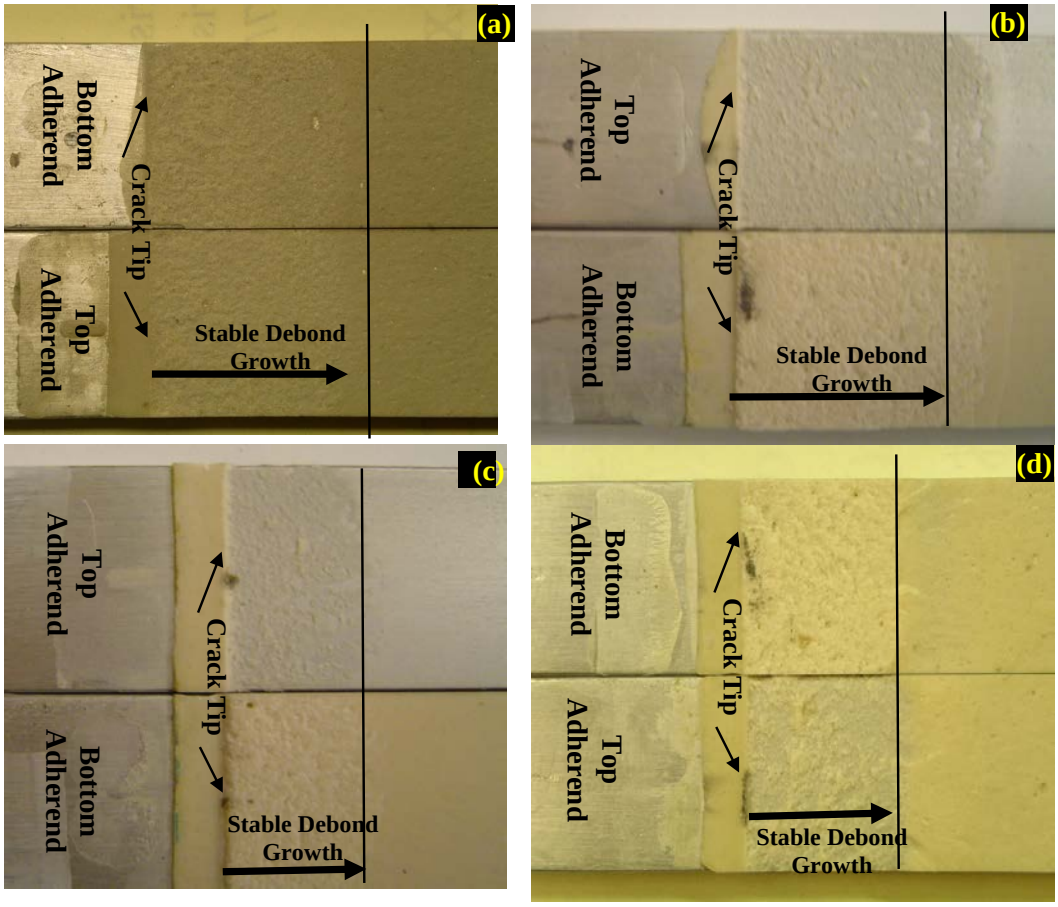

Figure 7. Fracture Surfaces for (a) Pure Mode I, (b) MMB 50%, (c) MMB 75%, and (d) Pure Mode II

As shown in the previous figures, there was a tendency for the debond to grow at the mid-plane of the adhesive layer for pure Mode I fracture. Thus, there was a uniform amount of adhesive remaining on both top and bottom adherends, as shown in figure 7(a). When a nonzero mode II component exists, the crack tended to turn and grow closer to the top adherend-adhesive interface, as evidenced in the MMB 50%, MMB 75%, and pure mode II fracture tests. Therefore, the amount of adhesive remaining on the top adherend, observed postfracture, was thinner compared to the bottom adherend, as shown in figure 7(b)-(d). This behavior was consistently observed throughout all experiments conducted and was also observed in references 8 and 14 during their pure mode II investigations.

3.3 CRITICAL STRAIN ENERGY RELEASE RATE RESULTS.

The CSERR is a global parameter used to calculate the crack's growth in the adhesively bonded joint, which describes the critical load associated with a material's fracture resistance. According to reference 22, an energy method approach instead of a stress-intensity factor is preferred for evaluating the fracture toughness of adhesively bonded joints because the CSERR is a global-based parameter that does not account for the contribution of compliance from the adhesive layer. Another advantage of this approach is that it can be used regardless of whether the crack propagates along the mid-plane or near the interface. Three different CSERR equations were employed to determine the CSERRs for fracture under pure mode I, mixed-mode, and pure mode II at fracture initiation.

The pure mode I CSERR (G_{I_C}) is derived from simple beam theory [16] and is shown in equation 1.

$$G_I = \frac{12P^2a^2}{B^2Eh^3} + \frac{4P^2}{B^2Eh} \tag{1}$$

where P is fracture load, a is crack length, B is specimen width, h is the thickness of the adherend, and E is the adherend Young's modulus.

The CSERR equations for mixed-mode fracture is also derived from beam theory and can be found in ASTM D 6671 [19]. The equations can be tailored for use with a desired mixed-mode ratio (G_{II}/G_{tot}) and is derived from superposition of mode I and mode II relationships [23]. The mode II component can be altered by changing the position c of the center roller away from the load point (see figure 2). The CSERR components used for the MMB 50% and MMB 75% tests are shown in equations 2 and 3.

$$G_I = \frac{12P^2(3c-L)^2}{16B^2h^3L^2E}(a+\chi h)^2 \tag{2}$$

$$G_{II} = \frac{9P^2(c+L)^2}{16B^2h^3L^2E}(a+0.42\chi h)^2 \tag{3}$$

where c is the arm length, L is the half span of the specimen, and χ is the crack length correction parameter. The total CSERR is given by equation 4.

$$G = G_I + G_{II} \tag{4}$$

The pure mode II CSERR relationship is shown in equation 5. This equation was used in references 10 and 12 to calculate the CSERR for pure mode II three-point bending fracture tests.

$$G_{II} = \frac{9P^2a^2}{16EB^2h^3} \tag{5}$$

By using the equations above with the fracture load determined from the experiments, the CSERR for various adhesive thicknesses can be calculated at fracture initiation. The CSERRs of pure mode I, MMB 50%, MMB 75%, and pure mode II are shown in figures 8 through 11. Pure mode I and MMB 50% show a similar CSERR versus thickness trend: the CSERR increased from 0.203- to 1.02-mm thickness and then dropped to a lower CSERR at 1.52-mm thickness. The rate of increase in CSERR is faster from 0.508 to 1.02 mm relative to the increase from 0.203 to 0.508 mm for both cases. MMB 75% tests show a relatively small variation of CSERR from 0.203- to 1.02-mm thickness in comparison to the other mixed-mode ratio cases. The CSERR also dropped to its lowest level (within the range investigated) at 1.52-mm thickness for MMB 75%. A different trend was observed for pure mode II fracture. The CSERR monotonically increased with bondline thickness, showing a linearly increasing trend from 0.203 to 1.02 mm, with a decreasing rate of increase from 1.02 to 1.52 mm.

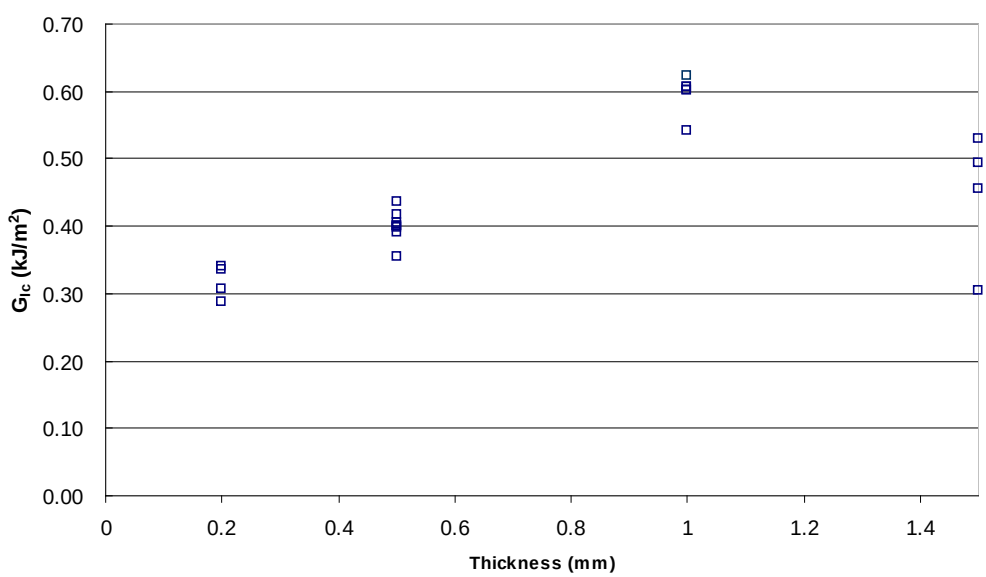

Figure 8. Pure Mode I CSERR (Initiation) vs. Adhesive Thickness

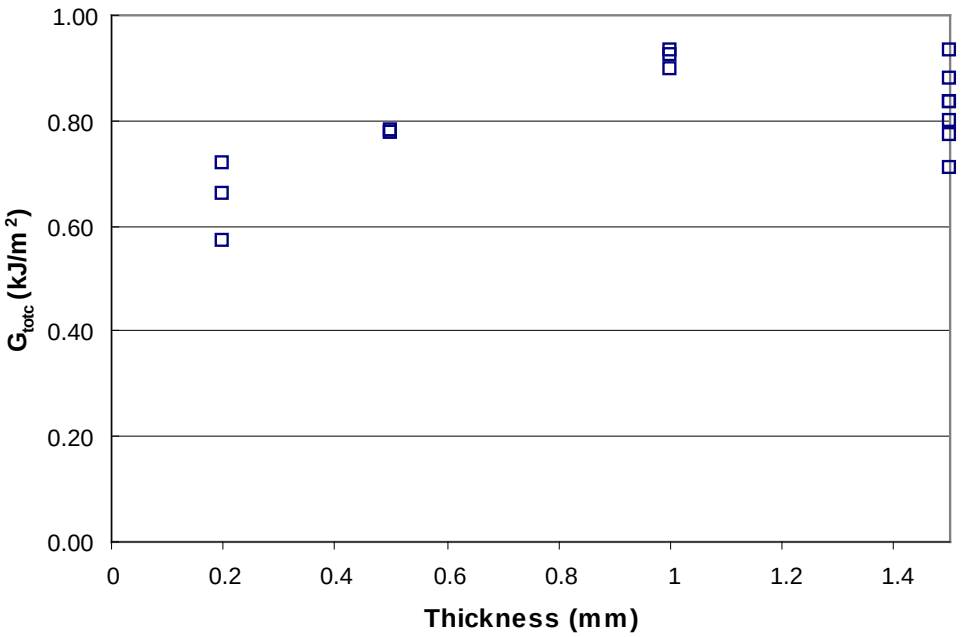

Figure 9. The MMB 50% CSERR (Initiation) vs. Adhesive Thickness

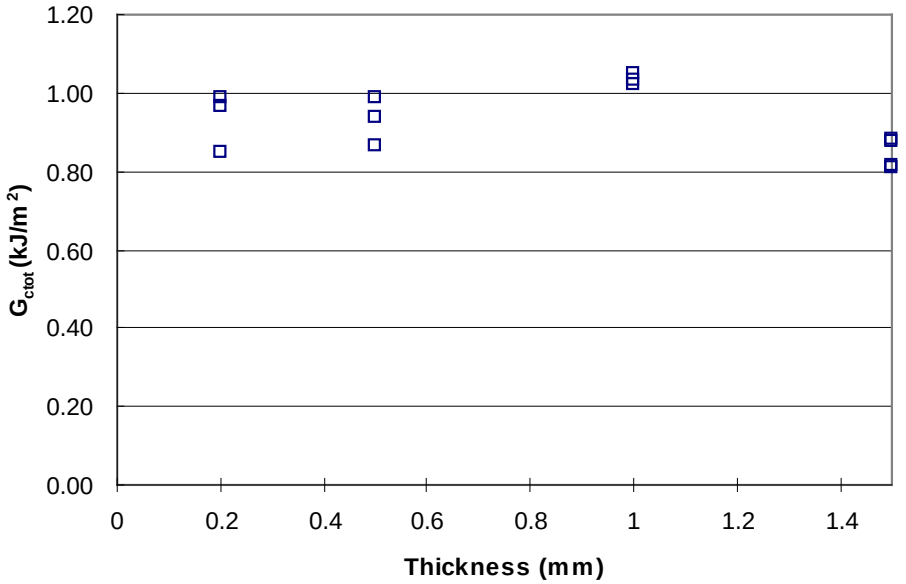

Figure 10. The MMB 75% CSERR (Initiation) vs. Adhesive Thickness

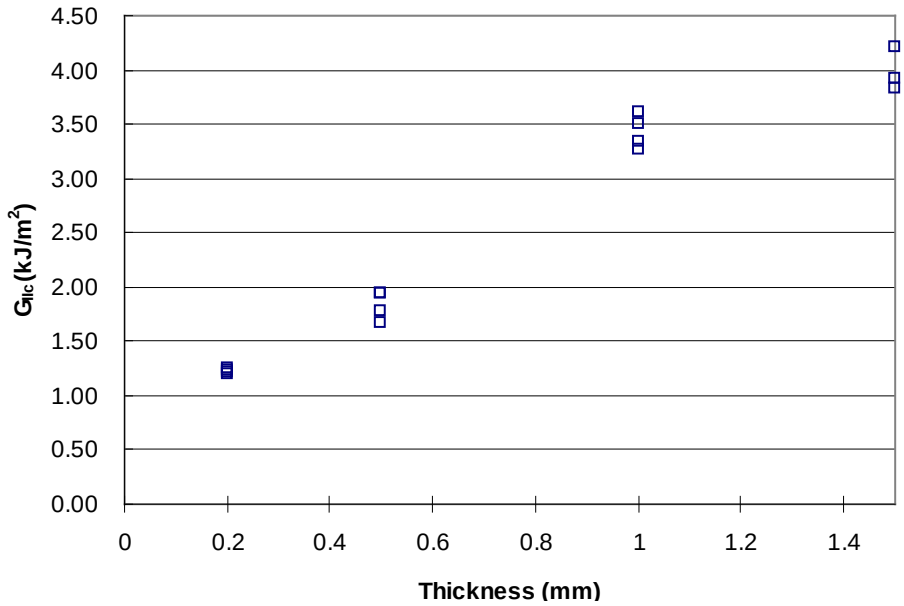

Figure 11. Pure Mode II CSERR (Initiation) vs. Adhesive Thickness

The plot of CSERR versus mixed mode ratio for all four adhesive thicknesses is shown in figure 12. A common trend of fracture energy versus mixed-mode ratio, regardless of the adhesive thickness, was observable: the fracture energy increases with higher mode II component. A similar trend was also encountered in the investigation of delamination for composite materials observed in references 6 and 7. It can also be observed in figure 12 that the rate of increase in CSERR was relatively small in the regime of low mode II ratio (for ratios less than 50%), while the CSERR significantly increased in the regime from mixed-mode 50% to pure mode II.

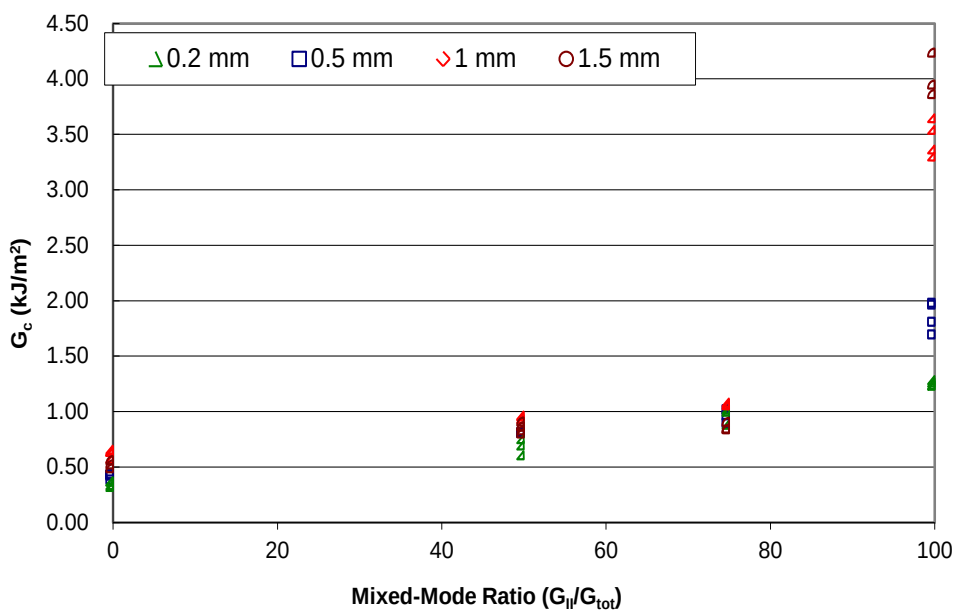

Figure 12. The CSERR (Initiation) vs. Mixed-Mode Ratio for Different Thicknesses

4. FINITE ELEMENT ANALYSIS.

4.1 MODEL DEVELOPMENT.

Finite element models were developed to investigate the shape and size of the plastic zone developed within the adhesive layer for different thicknesses and to correlate the trend of thickness-dependent CSERR measured experimentally. A commercial FEA code (ABAQUS®) was used in the analyses. Two-dimensional plane strain finite element models of the DCB, MMB 50%, MMB 75%, and ENF specimens were developed. They are similar in geometry to the experiment specimen except the pure mode I fracture model takes advantage of half symmetry. The adhesive thickness of each model is consistent with the actual adhesive thickness tested in the experiment, and the razorblade-defined initial crack tip geometry is exactly replicated. The material properties of aluminum 2024-T3 and PTM&W ES6292 epoxy adhesive were used, respectively, in the finite element modeling. Only the linear elastic behavior of the aluminum adherend was modeled, whereas the adhesive layer was modeled as behaving elastically up to the yield stress and behaving perfectly plastic thereafter. The material properties of the adhesive were determined from tensile test experiments of the bulk adhesive coupons [23]. Loads corresponding to experimentally measured critical loads were applied to the models. For the MMB specimens, the total load measured in the experiment can be decomposed to the equivalent components associated with mode I and mode II [24]. Plane strain quadrilateral elements (e.g., CPE8) were used to mesh all the FEA models. A reduced integration option was used in the pure mode II fracture model to reduce computational cost due to the larger overall size required to model the ENF test specimen.

4.2 THE FEA RESULTS.

Equivalent plastic strain in ABAQUS was used as the parameter (PEEQ) to determine the plastic zone size and shape at the time of fracture initiation, based on a cutoff level of 0.5% plastic strain. FEA predictions of plastic zone size and shape development in the adhesive layer at the time of fracture initiation for various thicknesses is shown in figures 13 through 16 for pure mode I, MMB 50%, MMB 75%, and pure mode II, respectively. The dimensions (length and height) of the plastic zone are indicated in each of these figures. Note that as the percentage of mode II content increased, the plastic zone size also increased. For pure mode II, the plastic zone was predicted to be the entire volume of adhesive contained between the crack tip and central roller.

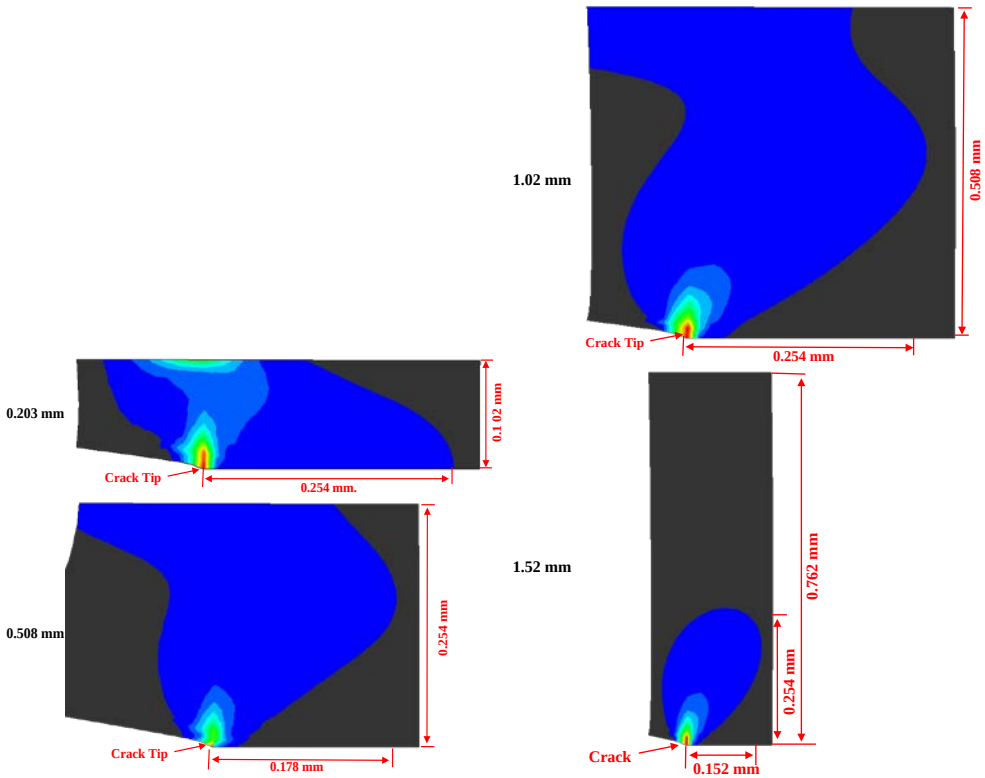

Figure 13. Comparison of Plastic Zone Size and Shape for DCB Pure Mode I

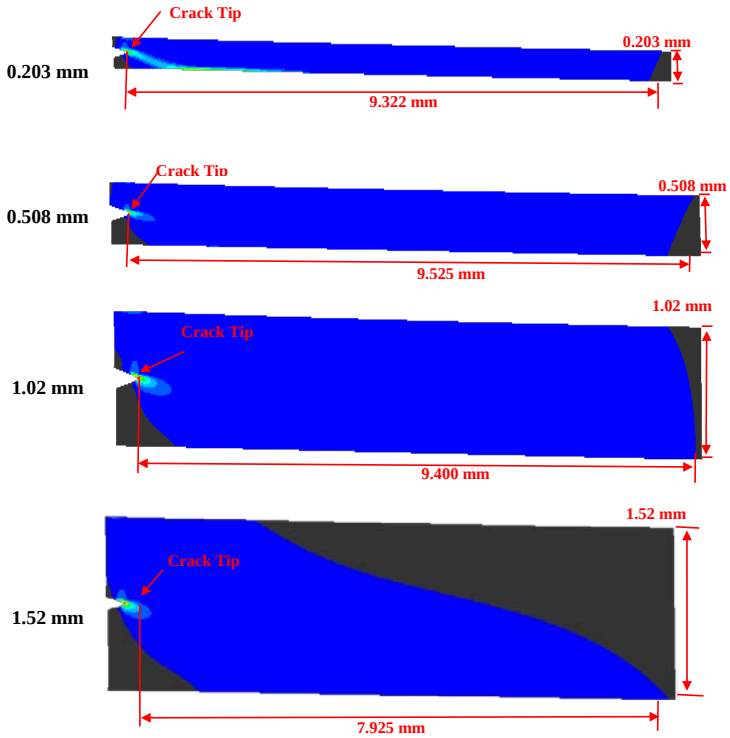

Figure 14. Comparison of Plastic Zone Size and Shape for MMB 50%

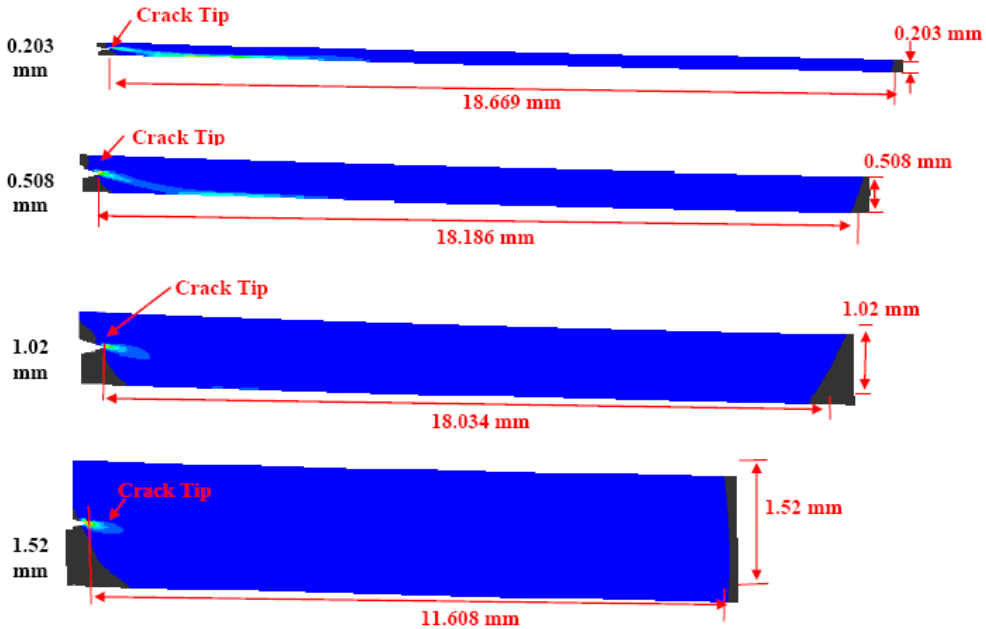

Figure 15. Comparison of Plastic Zone Size and Shape for MMB 75%

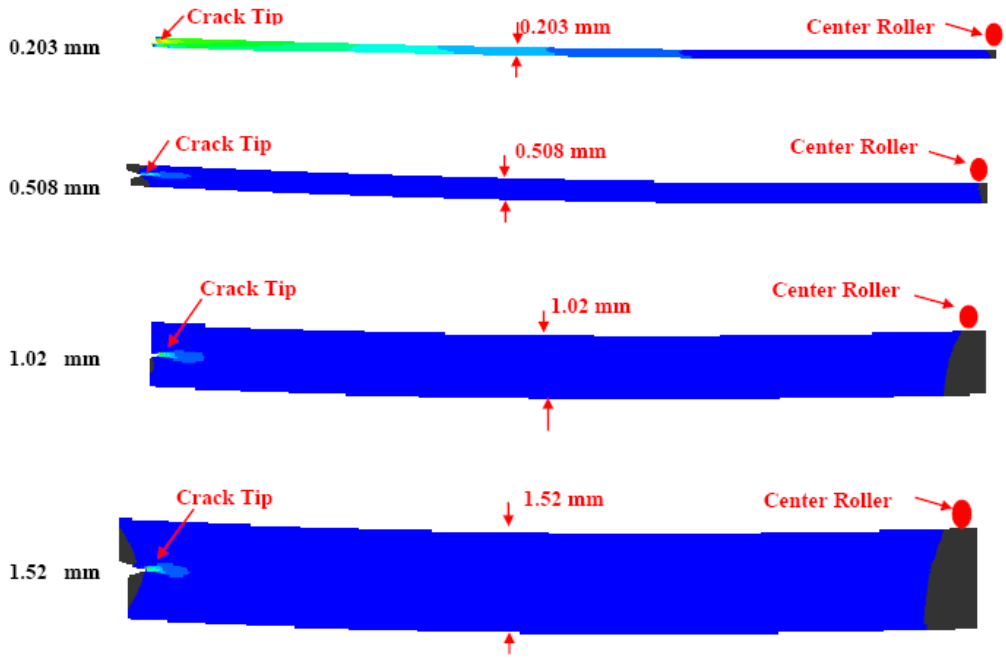

Figure 16. Comparison of Plastic Zone Size and Shape for ENF Pure Mode II

5. DISCUSSION.

For pure mode I, image 3 of figure 3 shows a very small crack growth at the crack tip when the load entered the nonlinear regime of the load displacement curve. Although a small crack is visible, the load still increased slowly but flattened at a peak level due to the joint compliance. For this small amount of cracking, a full-width crack front did not yet develop across the entire

specimen width, and thus, the joint was still able to carry increasing load. When the crack front developed across the full width of the joint, the load began to drop off as the function of increasing overall length. The crack propagated along the mid-plane of the adhesive layer in pure mode I fracture. A linear load displacement trend was observed at the beginning of the experiments, with larger nonlinear behavior observed prior to the onset of crack propagation. It is believed that the larger amount of nonlinearity observed for tests with higher mode II content is related to increased volume of adhesive that is being plastically deformed.

When a nonzero mode II fracture component existed, at roughly 90% of the fracture load, small crack growth was typically oriented at a specific angle relative to the initial crack, as shown in image 7 of figure 4, image 6 of figure 5, and image 7 of figure 6. Similar behavior was observed in references 11 and 14 in pure mode II fracture and in reference 24 for mixed-mode tests. The crack tended to run at a skewed angle until it came close to the interface and then propagated perpendicularly to the applied load near the adhesive interface with the top adherend. It is still valid to consider such fracture behavior as the measurement of fracture energy of the adhesive [11] instead of the measurement of adhesion fracture energy; this is because a significant amount of adhesive still remains on the adherend (cohesive failure), as shown in figure 7(b)-(d). Since the crack grows near the interface at the top adherend, the majority of the adhesive remains on the bottom adherend. It was claimed in reference 25 that the fracture energy of an asymmetric cohesive failure (kinked crack) is equal to the fracture energy of the central cohesive failure (mid-plane crack propagation). Although the compliance has changed during the crack growth initiation and orientation process, similar reasoning can be argued with the behavior observed in the pure mode I fracture specimens. Therefore, the maximum load was still used as the fracture initiation load to consistently define the fracture energy for all specimens tested and reported herein.

Figures 3 to 6 show that the scribe marks near the crack tip were skewed due to shear deformation resulting from the introduction of a mode II fracture component. The intensity of the skewing (shear) was not as visible for MMB 50% but was observed to increase with higher amounts of mode II. Figure 6 shows a closer observation that all six straight lines visible in the photographs, which span a distance of approximately 9.65 mm ahead of the crack tip, are skewed well before the onset of crack propagation. This is clear evidence that the plastic zone extends over a large region ahead of the crack tip [4]. Distortion of initially straight scribe lines was related as a measurement of local shear strain [11-13].

The failure mode for the mixed mode regime can be interpreted from the fracture surface, as shown in figure 7. It is evident that the failure surface of pure mode I loading yields a relatively smoother surface compared to pure mode II where a rougher surface can be clearly observed. For MMB 50% and MMB 75% specimens, the failure surfaces look quite similar to pure mode I. Based on this observation, it is believed that the mode I component is the dominant driving force controlling the onset of crack initiation and propagation for mode mix ratios at least up to 75%. Additionally, the mode II component plays a role to dissipate more energy by causing more volume of adhesive to plastically deform, and hence, the overall CSERR is higher with the existence of increased mode II component. The rough surface observed in these specimens can

also be attributed to the development and coalescence of microvoids, as was observed also in references 8, 10, 11, and 12.

From the experiments, there appears to be an optimum adhesive thickness that provides the highest CSERR for each mixed-mode ratio tested. Pure mode I and MMB 50% specimens show an increasing and then decreasing trend of CSERR versus bondline thickness. MMB 75% tests show a relatively flat relationship versus bond thickness. On the other hand, pure mode II tests show a monotonically increasing CSERR with increasing bondline thickness. In conjunction with the FEA results, it can be observed that the hypothesis posed in references 1 and 2, in which the CSERR is controlled by the plastic zone size, is applicable for the pure mode I and MMB 50% conditions. As observed in figure 13, the plastic zone for 0.203-, 0.508- and 1.02-mm joints interacts with the adherend, and therefore, the CSERR of joints with thicknesses ranging from 0.203 to 1.02 mm show an increasing trend. When the adhesive thickness is increased to 1.52 mm, the plastic zone does not interact with the adherend, and it occupies only one-third of the adhesive thickness for the pure mode I case. It is believed that the CSERR of the 1.52-mm adhesive thickness is approximately equal to the bulk adhesive's CSERR. It can be observed in figures 13 and 14 that the plastic zone length of MMB 50% fracture is much longer compared to pure mode I fracture. This increase in length is caused by the introduction of the mode II component. It can also be observed that the trend of CSERR correlated well with the plastic zone size arguments of references 1 and 2. The plastic zone interacts with the adherend when the fracture energy increases with adhesive thickness from 0.203 to 1.02 mm. However, as shown in figure 13, a significant volume of plastic zone no longer interacts with the top adherend. When the CSERR is lower than the maximum fracture energy, the plastic zone has less interaction with the adherends. Therefore, in pure mode I and MMB 50%, the plastic zone confinement by the adherend plays a role in the fracture toughness of the joints, as explained in references 1 and 2.

When the mode II component dominates, the correlation of critical energy release rate with the plastic zone size and shape becomes complicated because a larger volume of material is yielded by the dominant mode II, as observed in figure 15. Thus, no correlation between Kinloch's hypothesis [1-3] and the plastic zone size was found when the mode II ratio is dominant. As the mode II ratio increased to 100%, the entire volume of adhesive underwent yielding from the crack tip to the location near the center roller position, as shown in figure 16. This was expected, particularly when considering the large amount of shear deformation visible in image 10 of figure 6 (i.e., it has been shown that a very large plastic zone develops before the onset of crack propagation).

6. CONCLUSIONS.

The critical strain energy release rate, or G_c, of the adhesive system studied, PTM&W ES6292, exhibited strong bondline thickness dependency for pure mode I, mixed-mode bending (MMB) 50%, and pure mode II when exhibiting cohesive failure mode. Three different trends of G_c versus thickness were observed: (1) pure mode I and MMB 50% exhibits a peak value of G_c at 1.02-mm bondline thickness, (2) the trend for MMB 75% is nearly flat, and (3) G_c for pure mode II exhibited a monotonically increasing trend with bondlines increasing from 0.203 to 1.52 mm. Crack initiation tended to initially skew at an angle and grew near the top of the

adhesive-adherend interface when any amount of mode II component was present. However, the measurements are still considered the G_c of adhesive (as opposed to the interface) because the fracture failure mode was always cohesive. With a higher amount of mode II component, a larger-sized plastic zone developed in the adhesive layer, which resulted in a higher G_c being measured. The plastic zone size of the pure mode II specimens spanned the entire volume from the crack tip to the center roller. This was confirmed by both finite element analysis and experimental observations. The constraint of the plastic zone size and shape by the adherends was found to explain the bondline thickness dependency of G_c f or pure mode I and MMB 50% cases only, where G_c increased with bondline thickness until the plastic zone is no longer confined by the adherend. There was no plastic zone size correlation found for MMB 75% and pure mode II.

7. REFERENCES.

1. Kinloch, A.J. and Shaw, S.J., "The Fracture Resistance of a Toughened Epoxy Adhesive," *Journal of Adhesion*, Vol. 12, 1981, pp. 59-77.

2. Kinloch, A.J. and Moore, D.R., "The Influence of Adhesive Bond Line Thickness on the Toughness of Adhesive Joints," *The Application of Fracture Mechanics to Polymers, Adhesives and Composites*, ESIS Publication 33, 2003, pp. 149-155.

3. Hunston, D.L., Kinloch, A.J., and Wang, S.S., "Micromechanics of Fracture in Structural Adhesive Bonds," *Journal of Adhesion*, Vol. 28, 1989, pp. 103-114.

4. Chai, H., "Deformation and Fracture of Particulate Epoxy in Adhesive Bonds," *Acta Metallurgical et Matericlia*, Vol. 43, 1995, pp. 163-172.

5. Chai, H., "On the Correlation Between the Mode I Failure of Adhesive Joints and Laminated Composites," *Engineering Fracture Mechanics*, Vol. 24, 1986, pp. 413-431.

6. Benzeggagh, M.L. and Kenane, M., "Measurement of Mixed-Mode Delamination Fracture Toughness of Unidirectional Glass/Epoxy Composites With Mixed-Mode Bending Apparatus," *Composites Science and Technology*, Vol. 56, 1996, pp. 439-449.

7. Ducept, F., Davies, P., and Gamby, D., "Mixed Mode Failure Criteria for Glass/Epoxy Composite and an Adhesively Bonded Composite/Composite Joint," *International Journal of Adhesion & Adhesive*, Vol. 20, 2000, pp. 233-244.

8. Chai, H., "Shear Fracture," *International Journal of Fracture*, Vol. 37, 1988, pp. 137-159.

9. Chai, H., "Experimental Evaluation of Mixed-Mode Fracture in Adhesive Bonds," *Experimental Mechanics*, Vol. 32, No. 4, 1992, pp. 296-303.

10. Chai, H., "Micromechanics of Shear Deformations in Cracked Bonded Joints," *International Journal of Fracture*, Vol. 58, 1992, pp. 223-239.

11. Chai, H., "Observation of Deformation and Damage at the Tip of Cracks in Adhesive Bonds Loaded in Shear and Assessment of a Criterion for Fracture," *International Journal of Fracture*, Vol. 60, 1993, pp. 311-326.

12. Chai, H., "Deformation and Failure of Adhesive Bonds Under Shear Loading," *Journal of Material Science*, Vol. 28, 1993, pp. 4944-4956.

13. Chai, H., "Interfacial Mixed-Mode Fracture of Adhesive Bonds Undergoing Large Deformation," *International Journal of Solids and Structures*, Vol. 40, 2003, pp. 6023-6042.

14. Daghyani, H.R., Lin, Y., and Mai, Y., "Evaluation of Mode-II Fracture Energy of Adhesive Joints With Different Bond Thickness," *Journal of Adhesion*, Vol. 56, 1996, pp. 171-186.

15. Clearfield, H.M., McNamara, D.K., and Davis G.D., "Surface Preparation of Metals," *ASM Engineered Materials Handbook—Adhesives and Sealants*, Vol. 3, 1990, pp. 259-264.

16. ASTM International, "Standard Test Method for Fracture Strength in Cleavage of Adhesives in Bonded Metal Joints," ASTM D 3433-99, 2005.

17. Cavalli, M.N. and Thouless, M.D., "The Effect of Damage Nucleation on the Toughness of an Adhesive Joint," *Journal of Adhesion*, Vol. 76, 2001, pp. 75-92.

18. Blockman, B. and Kinlock, A., *Fracture Mechanics Testing Methods for Polymers, Adhesives and Composites*, Moore, D.R., Pavan, A., and Williams, J.G., eds., ESIS Publication 28, 2001, pp. 225-267.

19. ASTM International, "Standard Test Method for Mixed Mode I-Mode II Interlaminar Fracture Toughness of Unidirectional Fiber Reinforced Polymer Matrix Composites," ASTM D 6671/D 6671M, 2006.

20. Reeder, J.R. and Crews, J.R., "Mixed-Mode Bending Method for Delamination Testing," *AAIA Journal*, Vol. 28, 1990, pp. 1270-1276.

21. Tomblin J., Harter, P., Senevirante, W., and Yang, C., "Characterization of Bondline Thickness Effects in Adhesive Joints," *Journal of Composites Technology and Research*, Vol. 24, No. 2, 2002, pp. 332-344.

22. Kinloch, A.J., *Adhesion and Adhesives: Science and Technology*, Chapman and Hall, London, United Kingdom, 1987.

23. Lee, J., "Prediction of Adhesive Stress and Strain Solutions and Failure Criterion of Single Lap Bonded Joints," Purdue University Ph.D. Thesis, August 2006.

24. Chen, B., Dillard, D.A., Dillard, J.G., and Clark, R.L., Jr., "Crack Path Selection in Adhesively Bonded Joints: The Roles of External Loads and Specimen Geometry," *International Journal of Fracture*, Vol. 114, 2002, pp. 167-190.

25. Kawashita, L.F., Moore, D.R., and Williams, J.G., "The Measurement of Cohesive and Interfacial Toughness for Bonded Metal Joints With Epoxy Adhesives," *Composite Interfaces*, Vol. 12, No. 8-9, 2005, pp. 837-852.